

Reaction $^{27}\text{Al} + \alpha$ at $E_\alpha = 140$ MeV: II

W. F. Hornyak, M. D. Glascock,* C. C. Chang, and J. R. Wu

University of Maryland Cyclotron Laboratory, College Park, Maryland 20742

(Received 30 August 1978)

Both light and heavy mass fragments are observed giving angular distribution, energy, and particle identification information. Total cross section yields are compared to γ -ray-based values reported in the preceding paper. The mass fragment data are supportive of the γ -ray data particularly the observed Doppler broadening of the γ -ray lines. Comparison of the mass fragment and γ -ray data with both pre-equilibrium-evaporation and intranuclear cascade code predictions is discussed. Possible reaction mechanism models are discussed. Approximately 30% of the reaction cross section is assigned to direct processes, some involving collective surface excitations that appear to be memory conserving. Various possible direct pre-equilibrium processes are discussed.

NUCLEAR REACTIONS $^{27}\text{Al}(\alpha, x)$, $E = 140$ MeV; measured mass fragment $d^2\sigma/dE d\Omega$, deduce fragment velocities, Monte Carlo and exciton model calculations, deduce reaction mechanism model characteristics.

I. INTRODUCTION

Particle data on reaction products with $A \geq 4$ from 140 MeV α -particle incident on ^{27}Al were obtained in order to complement the inclusive γ -ray yield data and the results of an extensive study of the yield of very light particles $A \leq 4$.^{1,2} To permit cross section intercomparisons the mass fragments ($A \geq 4$) were observed down to low kinetic energies (~ 3 MeV).

The ultimate purpose of both the γ ray and mass fragment measurements was to determine the principal characteristics any successful reaction mechanism must possess and to compare the α -particle projectile results with the heavier ion results with projectile masses $A \geq 12$. The combination of spectroscopic information obtained from the γ -ray data in Ref. 1 with the mass fragment data greatly facilitates these studies.

II. EXPERIMENTAL METHOD

The mass fragments from a $520 \mu\text{g}/\text{cm}^2$ Al foil bombarded with 140 MeV α particles were detected in a 1.5 m diameter scattering chamber. Two movable detector arms and a multitude of different telescope elements and arrangements were used in relatively standard configurations. The combination of ΔE and E signals was used to determine the fragment charge and the measured flight time combined with E to determine the fragment mass. The best ΔE data was obtained with a $15 \mu\text{m}$ Si detector. Various E detectors ranging from $25 \mu\text{m}$ to 1 mm were used, each followed by a veto detector to eliminate transmitted high-energy,

light mass particles. The angular range $\theta_L = 10^\circ$ to $\theta_L = 135^\circ$ was covered using 5° intervals at the forward angles. Flight time information was obtained using the cyclotron beam fine structure. The timing resolution obtained was 3 ns. The cyclotron beam burst repetition time is 90 ns at $E_\alpha = 140$ MeV. Two separate flight paths were used: one with the longer path of 67 cm (the maximum permitted by the scattering chamber) to obtain good mass resolution for energetic particles and, one with a shorter path of 32 cm to permit seeing as low an energy as possible without a "wrap around" in the timing display. In this latter case a thin E detector of $50 \mu\text{m}$ thickness was used to permit vetoing any transmitted particles $A \leq 4$ (e.g., all α particles with $E > 8.1$ MeV and all protons with $E > 2.1$ MeV). The longer flight path data yielded unit mass resolution for the unfolded mass spectrum for $A \leq 16$, however, only a deteriorated resolution of about $\Delta M = 2$ was available at the $A = 30$ end of the mass distribution. Coupled charge and mass information were only obtainable for $A \leq 13$.

It was necessary to make substantial pulse-height defect and energy-loss corrections for the heavy mass fragments, $A > 4$, particularly at the lower energies. The pulse-height defect corrections were made using the prescriptions of Kaufman, *et al.*,³ employing a value for their "A parameter" of $A = 14$. This procedure and value of the A parameter gave satisfactory results even when applied to observed fission fragments in our detectors. The target energy-loss corrections were performed using the tables of Northcliffe and Schilling.⁴ All energies quoted in this paper refer to such corrected energies.

III. EXPERIMENTAL RESULTS

The observed relative angular distribution of all heavy mass fragments $A \geq 17$ was largely independent of the energy in the range $E > 7.5$ MeV. Figure 1 shows the absolute angular distribution for the integrated group of all fragments with $A \geq 17$ in the energy range $12.2 < E < 14.6$. To facilitate comparison with the γ -ray results which are angle-integrated results, we have plotted $d^2\sigma/d\theta_L dE$ ($\Delta E = 2.4$ MeV) versus laboratory angle θ_L . The result is a rather sharply peaked curve with a maximum near $\theta_L = 25^\circ$. As most relevant to angle-integrated results we show in Fig. 2 the observed relative mass spectrum obtained at the peak angle $\theta_L = 25^\circ$ for an energy slice $\Delta E = 0.48$ MeV centered at a mean energy $\bar{E} = 13.4$ MeV.

The energy spectrum above 4 MeV for the group consisting of all fragments $A \geq 17$ observed at $\theta_L = 30^\circ$ is shown in Fig. 3. The results for $A = 16$, 12, and 6 + 7 are also shown. We have also included for comparison the relevant data from Ref. 2 for α particles. If the exponential falloff evident at the higher energies is interpreted as an effective nuclear temperature relevant to energies measured in the laboratory frame, then the temperature (at 30°) is seen to decrease uniformly with increasing mass above $A = 4$. While the temperature rele-

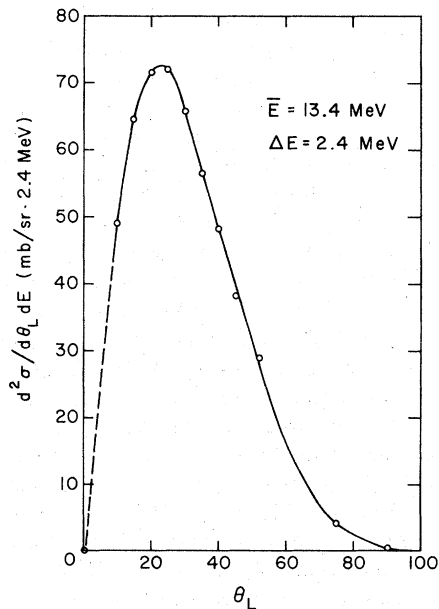


FIG. 1. The observed angular distribution, $d^2\sigma/d\theta_L dE$, for all mass fragments $A > 17$ within an energy window, $\Delta E = 2.4$ MeV, at a mean energy of $\bar{E} = 13.4$ MeV for the inclusive reactions $^{27}\text{Al}(\alpha, x)^A X$ at $E_\alpha = 140$ MeV. The energies quoted include pulse height defect and target energy loss corrections.

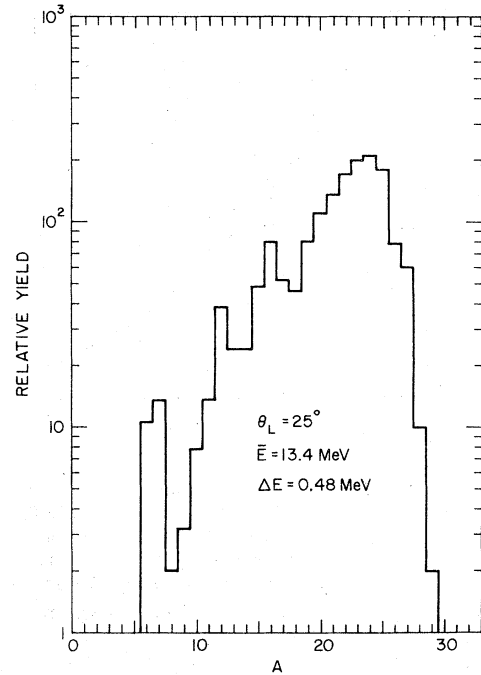


FIG. 2. The unfolded relative yield of mass fragments observed at $\theta_L = 25^\circ$, with an energy window $\Delta E = 0.48$ MeV, and corrected mean energy $\bar{E} = 13.4$ MeV.

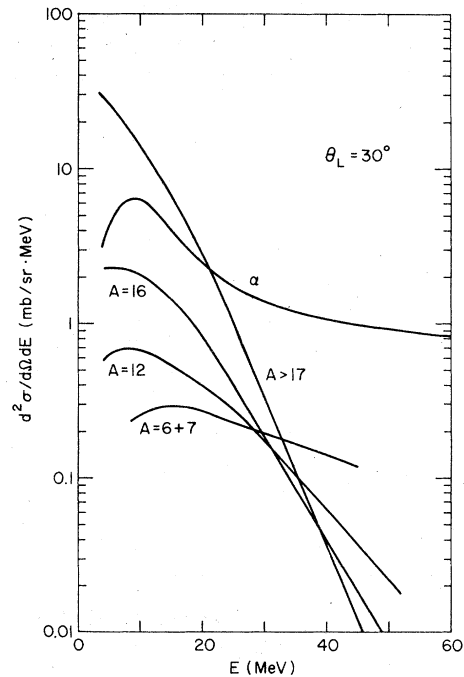


FIG. 3. The differential energy spectrum, $d^2\sigma/d\Omega dE$, observed at $\theta_L = 30^\circ$ for various mass fragments. The large number of experimental points with negligible statistical error are not shown. The major source of error associated with these curves results from the pulse height defect and target energy loss corrections particularly for $A \geq 12$ and $E \leq 5$ MeV. The estimated limit of error in energy for $A \geq 17$ at the lowest energy shown is $\pm 30\%$.

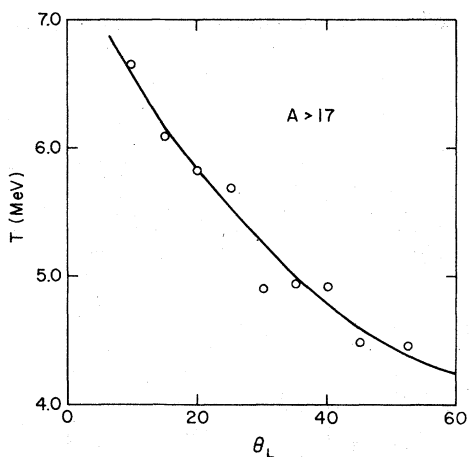


FIG. 4. The nuclear temperature for the mass fragments $A > 17$ as a function of the laboratory angle θ_L . The temperature is simple defined as the exponential factor T appearing in a Maxwell-Boltzmann form, $E \exp(-E/T)$, where E is in the laboratory frame. The value of T is derived for only the higher energy portion of the observed spectra.

vant to the high energy end of the spectrum for the fragments $A < 16$ is observed to be markedly angle dependent, this is not so much the case for $A > 17$. Figure 4 shows the variation of the effective temperature for $A \geq 17$ as a function of the angle θ_L .

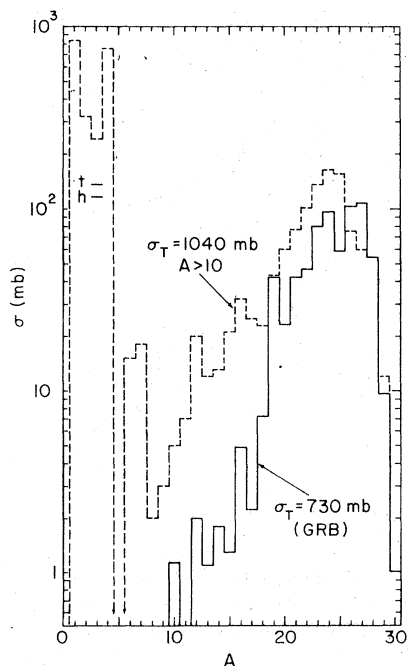


FIG. 5. The total energy and angle-integrated cross section for the inclusive production of the mass fragments A . For comparison, the gamma-ray based (GRB)-production cross sections are also included.

7 (N)						7	
6 (C)				0.3	0.7	18	5
5 (B)			2	W	4.5	6	2
4 (Be)			8	—	3	≤ 1	
3 (Li)			—	15	10	≤ 1	
2 (He)		111 [†]	756 [†]	—	?		
1 (H)	830 [†]	311 [†]	135 [†]				
0	—	?					
	0	1	2	3	4	5	6
	N						

FIG. 6. The total energy-and angle-integrated yield of a portion of the light mass isotopic fragments, based on both Z and A experimental identification. The associated error estimates for $A \geq 6$ are ± 1 mb. The entries marked with \dagger are from Ref. 2 taken under similar experimental conditions at $E_\alpha = 140$ MeV. The production of ^9B was assumed relatively weak based on the results given in Ref. 6.

The temperatures shown are for a simple Maxwell-Boltzmann fit, $E \exp(-E/T)$, where E is the laboratory fragment energy.

In order to obtain the desired angle- and energy-integrated mass spectrum, it is necessary to extrapolate the observed data such as shown in Fig. 3 to energies well below the lowest reliable experimental points at 3 or 4 MeV. To judge the importance of these extrapolations we should note that the fragments with $A \geq 17$ are deduced to have approximately 35% of the total cross section below 4 MeV in the laboratory frame. These extrapolations were made on the assumption that the broad low energy threshold apparent in the data is a real Coulomb barrier effect, as appears to be the case in the recent Berkeley data with 2–5 GeV protons on ^{27}Al .⁵ Calculated relevant Coulomb barrier energies of $E_c \approx 0.8, 2.6,$ and 4.2 MeV for $^{27}\text{Al}, ^{23}\text{Na},$ and ^{19}F were used. The effect of using these values is to reduce considerably the yields for low A fragments compared to those with high A . The final results for the total integrated cross sections are shown in Fig. 5. The entire cross section for $A \geq 10$ (possibly including some double counting below $A = 15$) is $\sigma_T = 1040$ mb. For the sake of completeness the observed results for the very light fragments $A \leq 4$ obtained by Ref. 2 are shown in Fig. 5. The γ -ray-based cross sections discussed in Ref. 1 are shown for comparison.

Figure 6 shows the total integrated isotopic yield for the lighter mass fragments $A \leq 13$. Again, for completeness results for $A \leq 4$ are also given.² The present results for $A \leq 13$ are in reasonable agreement in relative yields with earlier mea-

surements obtained for fragment energies greater than 25 MeV by Chant *et al.*⁶

IV. DISCUSSION AND CONCLUSIONS

This section is most conveniently divided into four parts, dealing with fragment velocity information, mass fragment yields, detailed calculated fits, and finally the inferred reaction mechanism characteristics.

A. Fragment velocities

The mean value of the laboratory frame kinetic energy (corrected for energy loss in the target) of the mass fragments $A > 17$ is relatively angle independent and has the value $\langle E \rangle = 8.4$ MeV at $\theta_L = 30^\circ$. If the transverse velocity component for the fragment ^{23}Na , selected as a probable example, is integrated over the angular distribution shown in Fig. 1, a mean value for $\beta_{\perp} = v_{\perp}/c$ of $\langle \beta_{\perp} \rangle = 8.0 \times 10^{-3}$ is deduced. The corresponding γ -ray Doppler broadening of $\text{FWHM} = 1.6 \times 10^{-2} h\nu_0$ is then calculated for unslowed-in-flight decay for this mean energy. For ^{23}Na γ rays with relevant level lifetimes $\tau_m \leq 100$ fs (i.e., short compared to stopping times) the observed Doppler broadening at 90° to the beam direction is $\text{FWHM} = 1.9 \times 10^{-2} h\nu_0$ (see Ref. 1), in satisfactory agreement with the above calculated value.

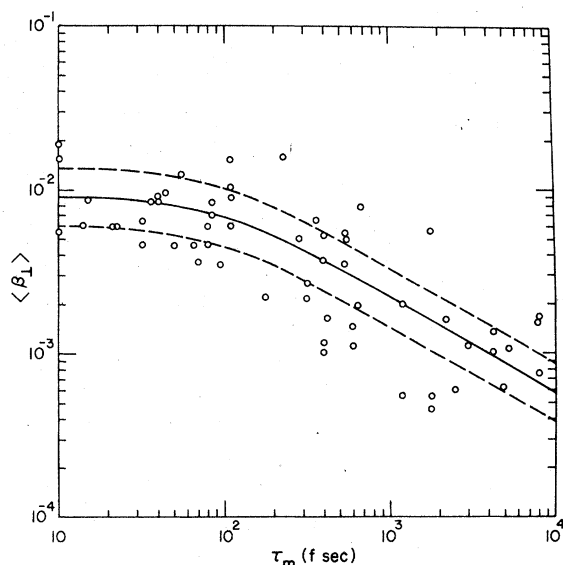


FIG. 7. The mean value of the transverse velocity $\langle v_{\perp}/c \rangle \equiv \langle \beta_{\perp} \rangle$ of the γ -ray emitting recoil mass fragments (determined from the observed Doppler broadening) as a function of the lifetime τ_m of the emitting level. The values were deduced from folding in both the observed energy and angular distributions of the fragments. The solid line and the dashed $\pm 50\%$ limits are only included to guide the eye.

Figure 7 shows the values of the mean transverse velocity $\langle \beta_{\perp} \rangle$ deduced for the various γ -ray lines discussed in Ref. 1 as a function of the mean emitting level lifetime. The selection has been limited to lines in nuclei with $A > 17$ that do not involve significant cascading. Because, as stated above, the energy distribution of these heavy fragments are quite similar, the asymptotic value of $\langle \beta_{\perp} \rangle \approx 9.0 \times 10^{-3}$ apparent in the figure for very short lifetimes may be considered consistent with the value specifically calculated for ^{23}Na . Slowing down in the $520 \mu\text{g}/\text{cm}^2$ target foil is also clearly evident in Fig. 7 for levels with longer lifetimes. The magnitude of the slowing down effect from the short lifetimes of $\tau_m = 10$ fs to the longer values of $\tau_m \approx (1-10)$ ps requires a substantial portion of the initial energy spectrum of the fragments to be below 2 MeV (the approximate range equivalent energy for the mean oblique foil thickness). This is consistent with the experimental results shown in Fig. 3 and the earlier cited extrapolation to lower energies suggesting a possible 35% yield below 4 MeV. As far as kinematic possibilities are concerned, the most probable energy and emerging angle for ^{23}Na fragments may equally well result from either the quasi-elastic scattering or the pre-equilibrium-evaporation process.

B. Mass fragment yields

The most striking feature of Fig. 5 contrasting the gamma-ray based (GRB) and directly detected mass fragment production cross sections is the increasing divergence between the two results as the fragment mass decreases. For fragment masses $A \geq 19$ there would appear to be of order 40% more cross section in the directly detected fragment yields than determined by the γ -ray data. Most of this difference may be ascribed to direct feeding of the ground states of the stable nuclei. Although any unobserved γ -ray cascading may also give a GRB cross section that is too low.

Below $A = 19$, strikingly more fragment production is evident than supported by γ -ray results. Of course, possible double counting below ^{15}N and still higher possible multiplicities particularly for $A \leq 7$ may be present. Generally, the possibility of failing to detect γ rays that may be present is somewhat higher for the lighter masses since they tend to have higher energy γ rays and also both shorter level lifetimes and higher velocities and therefore more Doppler broadening. However, in the case of the production of the residual nucleus ^{10}B , for example, the situation is unambiguous. All the particle stable levels and a majority of the particle unstable levels (including the giant resonances $12 < E_x < 18$ MeV) to the extent

that their γ decay have major decay branches through the first-excited state at 0.718 MeV with a lifetime of $\tau_m = 1.9$ ns. This γ ray is observed with a cross section of $\sigma_\gamma = 1.2$ mb. The only other significant γ -ray branch from the third-excited state with $E_\gamma = 414.8$ keV is not observed ($\sigma_\gamma \leq 0.5$ mb). The detected ^{10}B fragments give a cross section of $\Sigma = 4.5 \pm 0.8$ mb. (The possible error in extrapolating to the yield of low energy fragments is far less severe for ^{10}B than for the heavier fragments.) Thus, in this case the ratio of 3.8 for fragment to GRB yield must be judged real. Less compelling arguments for other light fragments also exist, leading to the general conclusion that ground state production of the light fragments is the dominant channel. This is in sharp contrast to the heavier fragments as mentioned above. For example, in the case of the production of ^{28}Al combining the prompt γ -ray data with the β -decay evidence gives a ratio of total yield to prompt GRB yield of only 1.2, implying only a 20% ground state feeding. The ratio of total yield to prompt GRB yield for ^{24}Na is 1.4, while for ^{20}F this ratio has risen to ≈ 3 .

Finally, the total GRB cross section of 730 mb and the total directly detected mass fragment cross section of 1040 mb for $A > 10$ should be contrasted to the calculated reaction cross section of 1148 mb. This calculated result is for a global optical model for ^{27}Al with interpolated parameters: $V_R = -107.5$ MeV, $r_{0R} = 1.28$ fm, and $a_R = 0.77$ fm for the real terms, and $V_I = -18.6$ MeV, $r_{0I} = 1.74$ fm, and $a_I = 0.495$ fm for the imaginary terms.

C. Calculated fits

Two separate model calculations are compared to the observed data pertaining to the total angle-integrated mass fragment yields. The first of these is for a model that employs a single pre-equilibrium stage followed by evaporation.⁷ Variants within this model are possible. We shall refer to such model calculations as PEEV (pre-equilibrium-plus evaporation). For a level density parameter $a = A/8$, an initial configuration of 4p-0h gives a somewhat better fit to the mass production data than an initial configuration of 5p-1h. The 4p-0h configuration does not, however, give the better fit to the spectra of the emitted charged-light particles (i.e., p , d , t , h , and α).² Further, it requires a separate *ad hoc* adjusted average nucleon-nucleon interaction matrix element to fit these light-particle spectra. The 5p-1h hole initial state does permit a constant matrix element and also results in a better fit to the light particles. The 5p-1h initial pre-equilibrium configuration, when coupled to a level density parameter, $a = A/20$, for the evaporation stage, gives as good a fit to

the heavier mass fragment data (i.e., $A \geq 6$) as any variant of this overall model. These results are shown in Fig. 8. While the most prominent yields are correctly predicted to be near $A = 24$, there is far too little production predicted for all masses with $A < 19$ except for the anomalously large yield for ^{16}O . This predicted anomaly also extends to ^{20}Ne and ^{24}Mg . These are considerably worse for the level density parameter $a = A/8$, where for example the predicted yield for ^{16}O increases to 149 mb from 88 mb with $a = A/20$. These values should be contrasted to the observed production cross section $\sigma = 32$ mb for all the $A = 16$ mass fragments (which is almost completely ^{16}O).

Figure 8 also shows a typical calculated result for a Monte Carlo type intranuclear cascade model developed in part by the chemistry group at the University of Maryland.⁸ This code, named CLUST, allows for possible pre-existing α -particle clusters in the target nucleus. It is a variant of VEGAS⁹ for the pre-equilibrium portion of the code using an eight-step nucleon density distribution to simulate any desired shape, for example, such as the standard Fermi shape. It employs the code EVA¹⁰ for the evaporation phase. α -particle nucleon scattering cross sections and initial mo-

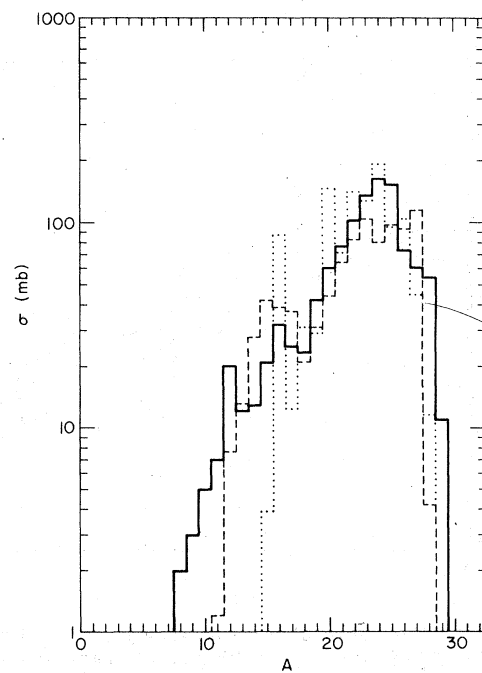


FIG. 8. Comparison between the observed total production cross section for mass fragments shown as the heavy solid line histogram, the PEEV model code results shown with the small dots, and the CLUST code prediction shown with long dashes.

TABLE I. Pre-equilibrium characteristics predicted by CLUST per cascade as a function of N_α , the number of pre-existing α -particle clusters in the target nucleus ^{27}Al . A total of 4000 cascades were run in each case.

N_α	0	1	2	3
Zero emitted particles	0.194	0.198	0.261	0.272
Avg. number of emitted n	0.313	0.239	0.298	0.265
Avg. number of emitted p	0.255	0.204	0.174	0.198
Avg. number of emitted α	0.519	0.481	0.415	0.394
Maximum collisions	14	16	20	24

mentum distributions for α -particle clusters when assumed to be present in the target nucleus are included in the program. The α -cluster density is taken to be proportional to the nucleon density.

Somewhat surprisingly the inclusion of pre-existing α -particle clusters *decrease* the pre-equilibrium emission of α particles. Several indicators given in Table I suggest that the presence of α clusters assists in moderating or degrading the incident α -particle energy more effectively, thereby permitting a rapid spreading of the energy among the nuclear constituents and thus have the system become more quickly equilibrated. This results simply from the well-known kinematic effect that elastic scattering from a comparable mass is the most effective means for energy loss.

To a remarkable extent the evident bias shown in Table I in the pre-equilibrium phase is almost all eliminated in the evaporation phase. At least for the presently used level density parameter $a=A/8$, the increased excitation of the evaporating nucleus as fewer particles are initially emitted in the pre-equilibrium phase results in a compensating larger evaporation phase emission. The variation over the entire $N-Z$ plane for $N_\alpha=0$ to $N_\alpha=3$ is less than 25% at most, there being somewhat more light mass production accompanied by somewhat less production near the target mass for $N_\alpha=0$ than the larger values of N_α . Figure 8 is for the case $N_\alpha=1$. It is evident from Fig. 8 that this cascade model produces a better overall fit to the experimental data than PEEV, particularly for the lighter masses. The peaking in the production yield near $A=16$ is now considerably (and more realistically) broadened.

A revealing comparison of the two models is shown in Figs. 9 and 10, where each prediction is compared to the observed angle-integrated cross section of emitted α particles taken from the data of Ref. 2. It is important to realize that the PEEV fit shown in Fig. 9 normalizes the pre-equilibrium yield to the data and that at most only one single pre-equilibrium particle is allowed to be emitted before beginning the evaporation phase. The curve labeled a is for the pre-equilibrium phase with the first cascade resulting in the emission of an

α particle, b for the total emission of pre-equilibrium α particles, and c for the evaporation component. The lack of high-energy α -particle emission referred to in Ref. 1 is evident. There is also a sizable hole in the predicted yield for $20 < E_\alpha < 60$ MeV.

Figure 10 shows the fit of the cascade calculation for $N_\alpha=1$ with no normalization to the data attempted. The curve labeled MODEL is for a Fermi density distribution with a radius parameter $r_0=1.07A^{1/3}$ fm and a central nucleon density of $\rho_0=0.1563$ fm $^{-3}$: a for the pre-equilibrium stage

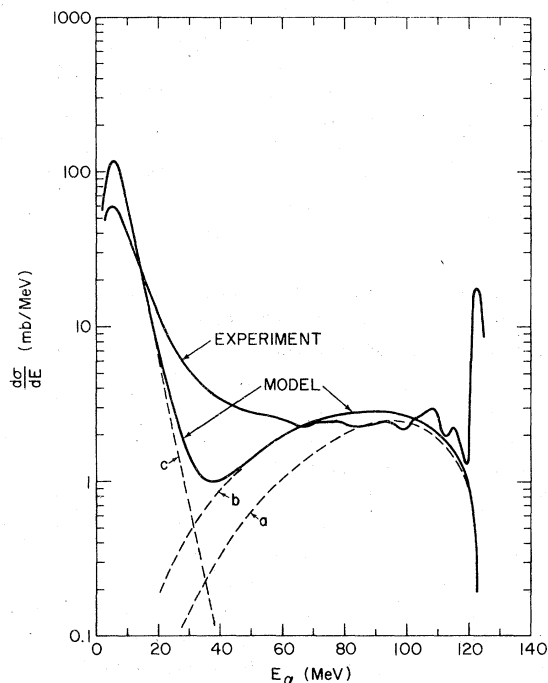


FIG. 9. The experimental angle-integrated cross section $d\sigma/dE$ for α particles compared to the pre-equilibrium and evaporation predictions of the PEEV model. The curve labeled (a) gives the pre-equilibrium component resulting from the very first interaction cascade; (b) gives the sum for emitted α 's resulting from all interaction cascades; and (c) is for the evaporation component. In this model the pre-equilibrium phase is ended when any pre-equilibrium cascade leads to the emission of a particle. All of these results are from Ref. 2.

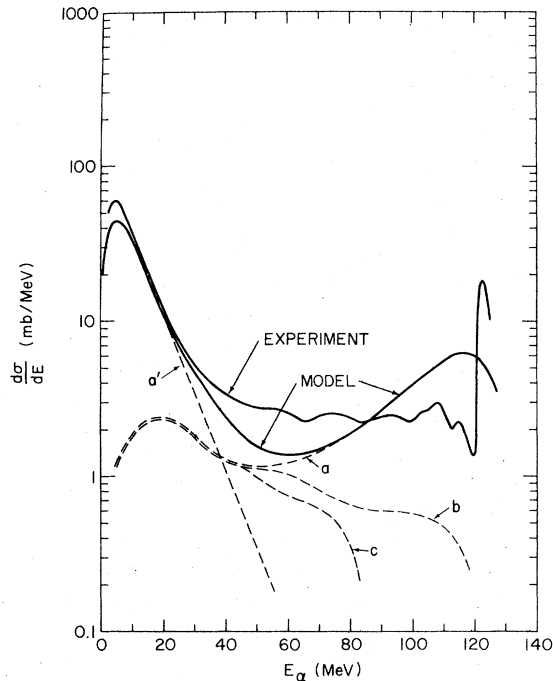


FIG. 10. The experimental angle-integrated cross section $d\sigma/dE$ for α particles compared to the pre-equilibrium and evaporation predictions for the CLUST code. The curve labeled MODEL is for the Fermi density distribution with a radius parameter $r_0 = 1.07A^{1/3}$ and a diffusivity parameter $a = 0.50$ fm: a, the pre-equilibrium and a', the evaporation components. The curve labeled b is the pre-equilibrium yield for a hard sphere nucleus with a radius $r_0 = 1.40A^{1/3}$ fm and curve c for a hard sphere nucleus with a radius $r_0 = 1.20A^{1/3}$ fm.

and a' for the evaporation stage. The significantly larger number of energetic pre-equilibrium α particles is attributed to the presence of the low nucleon density surface region permitting the α particles to interact and escape. The PEEV calculation does not consider surface density effects. Indeed, in contradistinction to the above result, the PEEV calculation² does fit the emitted proton spectrum quite well out to the highest energies due presumably to the longer mean free path of protons significantly reducing the importance of the surface effect. To exhibit the strong dependence of the high-energy yield in the pre-equilibrium phase on the nuclear density in the surface region, two additional density models were run with CLUST. In each case one pre-existing α -particle cluster was assumed. The curve labeled b in Fig. 10 is for a constant density hard sphere with $r_0 = 1.40A^{1/3}$ fm and a corresponding density $\rho_0 = 0.0935$ fm⁻³ and the one labeled c is for a hard sphere with $r_0 = 1.20A^{1/3}$ fm and $\rho_0 = 0.1382$ fm⁻³. Comparison of these curves clearly shows the increase in high energy yield with decrease in the

density in the surface region. Curiously enough the slight peaking in the yield near $E_\alpha \approx 20$ MeV appears not to depend on the above parameter variations.

As expected the total interaction cross section for the pre-equilibrium process decreases from 903 mb for the Fermi distribution to only 407 mb for the hard sphere case with a $r_0 = 1.20A^{1/3}$ radius. In the latter case the average number of α particles emitted per cascade also decreases to a value of 0.316.

The fact that the cascade model allows for multiple pre-equilibrium particle emission—until the separate cascade branches fall below the Coulomb barrier for charged particles or below the separation energy for neutrons—both cools the nuclei further and spreads the initial mass distribution at the start of the evaporation phase when compared to the PEEV model. The result is to partially fill in the hole for $20 < E_\alpha < 60$ MeV, populate lower mass final residual nuclei, and broaden the yield function near the α -particlelike nuclei ^{16}O , ^{20}Ne , and ^{24}Mg .

All values of N_α in the cascade model (Fermi density distribution) give essentially the correct value for the production cross section of ^{27}Al , predicting $\sigma = 100 \pm 10$ mb compared to $\sigma = 98$ mb for the GRB-experimental value. Unfortunately, the predicted result is almost completely for the α -particle emission channels from the initial configuration (i.e., $Z = 15$, $N = 16$). As discussed in Ref. 1, the entire angle-integrated observed (α, α') cross section leading to the production of ^{27}Al is approximately 40 mb and certainly less than 52 mb. We conclude that α -particle emission from the surface region is overestimated in the cascade model. It is unfortunate that the core capacity of the computer did not permit the inclusion of preformed triton clusters as well, since this might have produced the required pre-equilibrium damping of the α -particle emission. It is largely for the above reasons and to avoid double counting that only the PEEV calculation was cited in Ref. 1 relevant to the production cross section for $A = 27$ to 31. In any event both models omit complex direct processes that may be operating and in fact appear to be called for as we shall discuss later.

The experimental nuclear temperatures for the heavy fragments shown in Fig. 4 may be translated into excitation energy of the initial emitting system, using the approximate relationship $E_x \approx aT^2$ with $a \approx A/8$. We obtain for the laboratory angle with largest $d^2\sigma/d\theta_L dE$ a temperature $T(\theta_L = 25^\circ) = 5.4$ MeV and an excitation $E_x \approx 100$ MeV. For the intranuclear cascade model CLUST this corresponds to the average excitation for the pre-equilibrium state resulting from the emission

of a single nucleon. The temperature at the most forward heavy fragment angle $T(\theta_L = 10^\circ) = 6.5$ MeV yields the complete fusion excitation of $E_x \approx 140$ MeV. An extrapolated temperature of $T \approx 4.0$ MeV for heavy fragments emitted at angles greater than 60° yields an excitation energy of $E_x \approx 50$ MeV, a value close to the predictions of CLUST for pre-equilibrium residuals of $A \approx 24$ to 26.

An insufficient matrix of observed laboratory energies and angles prevents energy spectra, temperatures, etc., from being determined at various fixed center of mass emission angles. Incidentally, the mean laboratory energy of $\langle E \rangle = 8.4$ MeV at a laboratory angle of 30° translates to an energy of 3.4 MeV and angle of 128° in the c.m. frame.

D. Inferred possible reaction mechanism

The major features of the results discussed in both this paper and in Ref. 1 that must be considered in any model for the reaction mechanism are:

(i) The strong implication of the γ -ray data for all of the heavy mass nuclei is that there is significant nuclear particle feeding of levels by direct processes, some apparently also involving collective excitations. The reference here is to the striking result that the most strongly excited states in all the residual nuclei appear to have a collective parentage to rotational states of the target that involve coupling a quadrupole phonon of excitation to the target ground state. The numerous specific cases are discussed in Ref. 1. The total cross section for such processes is estimated to be $\sigma \approx 300$ mb or about 30% of the total reaction cross section. This value is obtained by summing the excess feeding of these direct excited states above an average production cross section value obtained from the excitation of all of the other remaining levels.

(ii) The observation that most of the resulting γ rays from the above process are severely Doppler broadened requires momenta possible only by the recoiling of the heavy fragment from the emission of a few energetic light fragments as opposed to possible numerous sequential low-energy nucleon evaporation steps.

(iii) The failure to observe de-excitation γ rays in the light fragments $6 \leq A \leq 18$ with comparable cross sections to the observed corresponding fragment yields, suggests largely ground state production.

(iv) The observed cross section for mass fragments with $6 \leq A \leq 11$ is 50 mb. The production of these nuclei compared to their complimentary heavy fragment masses $(31-A)$ give an average ratio $\langle \sigma(A)/\sigma(31-A) \rangle \approx \frac{1}{11}$ with a variation of less than a factor of 2 for individual values of A . Neither the PEEV code nor the CLUST code give adequate

yield below a fragment mass $A = 12$.

The overall description of the possible reaction mechanisms involved are perhaps best discussed in terms of the impact parameter in the incident channel. For large impact parameters or grazing collisions, strong direct processes may be expected possibly involving surface cluster components. The γ -ray data discussed in Ref. 1 offer evidence of just such processes very selectively involving particular states. These occur in all the even-odd nuclei for which individual γ -ray assignments were possible, namely, ^{15}N , ^{15}O , ^{19}F , ^{21}Ne , ^{23}Ne , ^{23}Na , ^{25}Mg , ^{25}Al , ^{29}Si , as well as ^{27}Al . In all cases only certain of the $(\frac{3}{2}, \frac{5}{2}, \frac{7}{2}, \frac{9}{2})^+$ levels are involved. For many of these the literature offers evidence of 3p-3h state components with the three particles in the $2s1d$ shell. In other cases conjecturing the same possibility does not involve any particular difficulty.

For the even-even $2s1d$ -shell nuclei: ^{20}Ne , ^{22}Ne , ^{24}Mg , ^{26}Mg , and ^{28}Si , the largest observed cross sections feed the lowest 2^+ levels in each case, even after all γ -ray cascading through these states have been corrected for. The direct processes leading to these states may thus involve simultaneous excitation of a quadrupole phonon. The evidence for ^{27}Al , ^{25}Mg , ^{25}Al , ^{23}Na also suggest strong direct processes accompanied by a quadrupole phonon excitation.

A unified model which allows for both particle emission and transfer of particles between colliding ions as well as the simultaneous excitation of collective surface modes is that proposed by Broglia, Winther, and collaborators^{11,12} and particularly the most recent advances.¹³ Although originally proposed for heavy ion reactions, we suggest the possibility that under present experimental conditions a similar model has some applicability for incident alpha particles as well. Figure 11 is a schematic semiclassical illustration of the situation following Broglia.

For large impact parameters or grazing collisions, quasi-elastic processes would be expected that simultaneously excite collective surface oscillations that are memory conserving. Thus, collective modes in the heavy fragments would be generically related. In the present instance a collision time $\tau_{\text{coll}}/\hbar \approx 0.2$ MeV⁻¹ may be estimated. Collective quantum transitions of order $\Delta E \approx 5$ MeV would thus be expected to dominate for such collisions. Thus quadrupole excitation of lower lying states should be strong. The latter is just what is needed for item (i) above. The γ -ray data clearly suggest strong feeding of such states.

Although discussed in detail in Ref. 1, the salient points briefly cited are perhaps in order here. The strong excitation of the 2^+ first excited states in ^{26}Mg and ^{28}Si may be assumed to be simple nu-

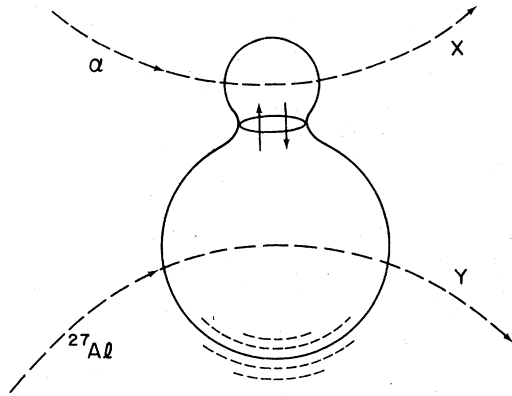


FIG. 11. A schematic semiclassical representation of the Broglia and Winther model showing a peripheral interaction of the α particle and ^{27}Al target. The diffusion window shown in the overlap region occurs when the potential barrier between the two systems is lowered sufficiently below the Fermi energies to allow nucleons to diffuse between the two systems. Importantly, surface vibrations in one or both systems are simultaneously excited.

neon transfers into or out of the $\frac{5}{2}^+[202]$ Nilsson orbital plus a quadrupole phonon excitation. The levels of ^{25}Mg relatively strongly excited are the first four (up to the point where the level order in ^{25}Mg and ^{27}Al no longer track). The ratio of the feeding cross section of these ^{25}Mg levels to the corresponding ones in ^{27}Al are sensibly constant with $Y(\text{Mg})/Y(\text{Al}) = 0.5$ within experimental errors. Simple transfer or knockout processes involving a neutron and proton pair from this same Nilsson orbital might account for this result.

If the mechanism described above does in fact correspond to the mode of excitation of these heavy recoil fragment states, the Doppler broadening referred to in (ii) above would automatically follow. This would also be consistent with not requiring γ -cascading to be the main source of populating these states.

We might inquire about the state of the lighter fragments associated with the 300 mb or so cross section of the direct quadrupole excitation of the heavy mass fragments. Both the characteristics contained in (iii) and (iv) above may be accounted for by the assumption of a light fragment spallation shower emission involving masses $A \leq 4$. Favorable spallation fragment condensation into a single complementary mass to the heavy fragments is required by the data to occur of order $\frac{1}{6}$ of the time to account for the observed 50 mb production cross section for $6 \leq A \leq 12$.

At small impact parameters the incident particle generally would be expected to undergo collisions leading to complete momentum transfer, thus facilitating fusion-like processes leading in

the equilibrated limit to compound nucleus formation. Correcting the observed heavy fragment yield of Fig. 5 for the 300 mb cross section of direct processes discussed earlier results in an essentially similar mass distribution. Most of the cross section is again in the mass range $21 \leq A \leq 29$ with a broad peak at $A \approx 25$. Interestingly, this mass distribution is quite similar to that observed for ^{19}F ions on ^{12}C at E_x (c.m.) = 52 MeV and attributed to the fusion process.¹⁴ In that experiment the mass spectrum also ranged from $21 \leq A \leq 29$ with a broad peak at $A \approx 25$. Both experiments indicate similar fragment energies in the center-of-mass frame.

In the ^{19}F ion experiment¹⁴ the fusion cross section is determined to be $\sigma_F = 1070$ mb. If in the present experiment we also designate the corresponding corrected spectrum as fusion we arrive at

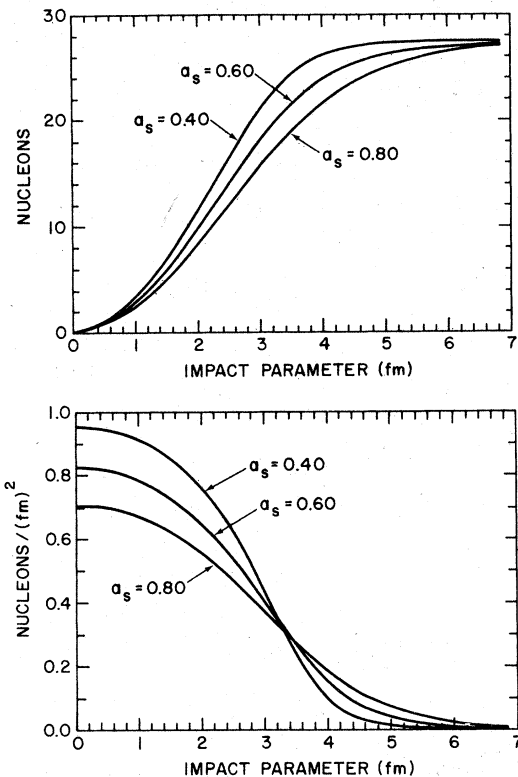


FIG. 12. (a) The nucleon density for ^{27}Al projected onto a plane perpendicular to the α -particle incident direction, in terms of the impact parameter. The curve is for a Fermi spherical distribution with a radius parameter $r_0 = 1.18A^{1/3}$ fm and three surface diffusivity parameters, $a_s = 0.40, 0.60,$ and 0.80 fm. (b) The total nucleon number for the above situation, from an impact parameter zero up to the value shown. The fraction of the number of total nucleons outside an area defined by an impact parameter equal to the three-dimension half-density radius (3.54 fm) is 0.319, 0.222, and 0.126 for $a_s = 0.80, 0.60,$ and 0.40 fm, respectively.

$\sigma_F \approx 800$ mb at $E_x(\text{c.m.}) \approx 100$ MeV. This estimate of 800 mb results from subtracting the observed total excess direct excitations of 300 mb, augmented by an estimated 20% to allow for unobserved ground state production, from the calculated reaction cross section of $\sigma_R = 1150$ mb. In the present context, ordinary pre-equilibrium emission and evaporation processes of the type included in PEEV and CLUST are arbitrarily attributed to fusion and compound nucleus production. It is difficult to know how to allow for other pre-equilibrium processes without double counting. We have, for example, required some of the known α particle breakup process¹⁵ to provide the missing cross section for the quadrupole excitations in the residual ^{27}Al nucleus.

The higher relative velocity in the present case, both due to the elevated energy and the lighter mass incident projectile results in a collision time τ_{coll} that is only $\frac{1}{4}$ of that for the heavier ion reaction. Presumably this shorter time for accommodation to a fusion state accounts for some of the difference. Another factor that enters in the comparison involves the projected nucleon densities. A ready interpretation applicable at very high energies might also be suggestive even at the present energy of $E_\alpha = 140$ MeV. Figures 12(a) and 12(b) show the projected nucleon density per square Fermi and the total number of nucleons as functions of the impact parameter for three different surface diffusivities, $a_s = 0.40, 0.60,$ and 0.80 fm.¹⁶ An α particle considered as a single projectile with a radius of 1.2 fm passing directly through the target nucleus center following a classical trajectory encounters only 3 to 4 nucleons within its projected geometric area. The ^{27}Al nucleus is thus seen to be a rather rarified nucleon cloud for a small-sized integral projectile. On the other hand, a direct central collision of a ^{19}F and a ^{12}C nucleus would immediately involve all 31 nucleons in the resulting interaction. It is also relevant to notice that for ^{27}Al the surface zone extending from an impact parameter equal to the (three-dimensional) half-density point to infinity contains as much as 32% of the nuclear matter for the larger diffusivity of $a_s = 0.80$ fm. This allows for an ample fraction of the $^{27}\text{Al} + \alpha$ interactions to be of the surface encounter variety.

E. Near symmetric breakup modes

The conspicuous local peaks in the observed mass fragment spectrum near $A = 12$ and 16 require comment. In addition to the major yield involving multiple α particle, triton, and nucleon emission by ordinary pre-equilibrium and evaporation processes of the type discussed above,

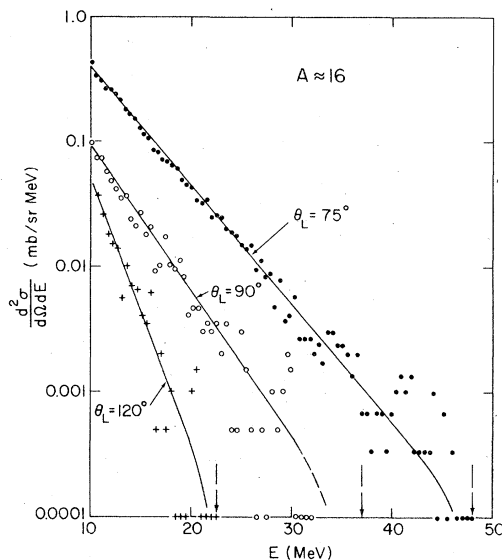


FIG. 13. The high-energy portion of the energy spectrum of $A = 16$ mass fragments at $\theta_L = 75^\circ, 90^\circ,$ and 120° . The asymptotic values $E_F = 48.0, 37.1,$ and 22.6 MeV for near symmetric breakup, $^{27}\text{Al}(\alpha, ^{16}\text{O})^{15}\text{N}$, are also shown.

the speculative possibility exists for near symmetric breakup of the compound system. It is unlikely for this to be the result of a classical fission (equilibrated) process from the fusion state with the transfer of the full incident momentum and the resulting large internal excitation. Some form of quasifission (unequilibrated) leading to the reaction $^{27}\text{Al}(\alpha, ^{16}\text{O})^{15}\text{N}$ might be possible, as well as quasifission of the target nucleus in an incomplete momentum transfer process such as $^{27}\text{Al}(\alpha, \alpha')(^{12}\text{C} + ^{15}\text{N})$. Alternatively, heavy particle knockout of either the entire p -shell core or a portion of it, exists as another possibility. Although the Q value for the $(\alpha, 4\alpha)$ process leading to the formation of ^{15}N is favorably small, $Q = -24.6$ MeV, the Q value for near symmetric breakup is even more favorable, being only $Q = -10.1$ MeV. The Q value for the above incomplete momentum quasifission is $Q = -17.4$ MeV. Even quasifission following a pickup process such as the reaction $^{27}\text{Al}(\alpha, ^7\text{Li})(^{12}\text{C} + ^{12}\text{C})$ does not represent too large a Q -value penalty in comparison to $(\alpha, 4\alpha)$, being only $Q = -29.7$ MeV.

In Fig. 13 the high energy portion of the recoil mass $A = 16$ (mostly ^{16}O) is shown for laboratory angles $\theta_L = 75^\circ, 90^\circ,$ and 120° . The asymptotic end point energies for the process $^{27}\text{Al}(\alpha, ^{16}\text{O})^{15}\text{N}$ (leaving both fragments excited to typical bound state energies) are also shown. The data appear to approach these asymptotes albeit with very low cross sections. The similar process involving inelastic α -particle excitation, of course, would

offer the possibility of lower recoil energies as well. Incidentally, the maximum energy a recoiling ^{16}O ion would have if it were an elastically scattered oxide contaminant nucleus on the target surface would be only 6.0 MeV at $\theta_L = 75^\circ$, and, of course, could not appear at all for the angles $\theta_L = 90^\circ$ or 120° . It is with this in mind that only the large angle data are shown. It should also be remarked that the only prompt γ radiation observed from ^{16}O and the mirror nuclei ^{15}O and ^{15}N are from the unnatural parity states, 3^- and $\frac{5}{2}^+$, respectively. In any event states with known prominent $3p-3h(2s1d)^3$ configuration components are excited in all three cases, see Ref. 1. If the near symmetric breakup processes result from memory conserving mechanisms, it might be expected that such $(2s1d)^3$ configurations would be preferentially excited, since it is present in the target nucleus.

Thus, evidence does exist for near symmetric breakup of the incident configuration. If the entire yield of mass $A = 15$ and 16 above a laboratory kinetic energy of 30 MeV is attributed to such processes, a yield of order $\sigma_B \approx 2$ to 5 mb results. The γ -ray cross sections for ^{16}O , ^{15}O , and ^{15}N cited above are of comparable magnitude, being 4.0, 0.2, and 1.1 mb, respectively.

The mass peak near $A = 16$ also appears in the

data of Ref. 14 for ^{19}F ions incident on ^{12}C . That reference, however, attributes the majority of these events to breakup of the ^{19}F projectile. This is quite likely the case, since the fusion state with an excitation of 52 MeV would not be expected to undergo classical fission compared to other decay channels. Thus the quasifission process, if present, is unique to the present experiment.

Finally, we should remark on the overall success, albeit of not too great accuracy, of both the code calculations PEEV and CLUST in fitting the mass fragment data both in mass distribution and total yield. It is suggested that this may be another example of the success of simple statistical models in accounting for events averaged over the subtleties of microscopic models. Error free handling of kinematics and the inclusion of experimental Q values plus the genuine applicability of the model to a major portion of the reaction mechanism may account for the success observed.

We wish to thank N. S. Wall, B. G. Glagola, and H. D. Holmgren for many useful discussions. A grant from the University of Maryland Computer Science Center for carrying out some calculations is acknowledged. This work was supported in part by the National Science Foundation.

*Present address: Research Reactor Facility, University of Missouri, Columbia, Missouri 65201.

¹M. D. Glascock, W. F. Hornyak, C. C. Chang, and R. J. Quickle, preceding paper.

²J. R. Wu, C. C. Chang, and H. D. Holmgren, Phys. Rev. C **19**, 659 (1979).

³S. B. Kaufman, E. P. Steinberg, B. D. Wilkens, J. Unik, A. J. Gorski, and M. J. Fluss, Nucl. Instrum. Methods **115**, 47 (1974).

⁴L. C. Northcliffe and R. F. Schilling, Nucl. Data Tables **7A**, 233 (1970).

⁵G. D. Westfall, R. G. Sextro, A. M. Poskanzer, A. M. Zebelman, G. W. Butler, and E. K. Hyde, Phys. Rev. C **17**, 1368 (1978).

⁶N. S. Chant, J.-P. Didelez, B. T. Leemann, H. G. Pugh, and N. R. Yoder, Univ. of Maryland Progress Report (1974) (unpublished), p. 36.

⁷J. R. Wu and C. C. Chang, Phys. Rev. C **17**, 1540 (1978).

⁸R. A. Moyle, G. J. Mathews, B. G. Glagola, and V. E. Viola, private communication.

⁹K. Chen, Z. Fraenkel, G. Friedlander, J. R. Grover, J. M. Miller, and Y. Shimamoto, Phys. Rev. **166**, 949 (1968).

¹⁰I. Dostrovsky, Z. Fraenkel, and G. Friedlander, Phys. Rev. **116**, 683 (1960).

¹¹R. A. Broglia and A. Winther, Phys. Rep. **4C**, 153 (1972).

¹²R. A. Broglia, C. H. Dasso, and A. Winther, Phys. Lett. **53B**, 301 (1974); **61B**, 113 (1976).

¹³R. A. Broglia, Bull. Am. Phys. Soc. **23** (No. 4), 550 (1978).

¹⁴R. Pühlhofer, W. Pfeffer, B. Kohlmeyer, and W. F. W. Schneider, Nucl. Phys. **A244**, 329 (1975).

¹⁵J. R. Wu, C. C. Chang, and H. D. Holmgren, Phys. Rev. Lett. **40**, 1013 (1978).

¹⁶R. Koontz and H. D. Holmgren, private communication.